Investigation of Charge Transport in Amorphous $Ge_2Sb_2Te_5$ Using the Variable-Range Hopping Model

Enrico Piccinini, Fabrizio Buscemi,
Thierry Tsafack and Massimo Rudan
"E. De Castro" Advanced Research Center on Electronic Systems
and Department of Electronics, Computer Science and Systems
University of Bologna
Viale Risorgimento 2, I-40136 Bologna, Italy
Email: enrico.piccinini@unimore.it

Rossella Brunetti and Carlo Jacoboni
Physics Department and
CNR-INFM National Research Center on
nanoStructures and bioSystems at Surfaces (S^3)
University of Modena and Reggio Emilia
Via Campi 2137A, I-41025 Modena, Italy
Email: rossella.brunetti@unimore.it

***Abstract*—Chalcogenide GST materials can suitably be exploited for manufacturing phase-change memory devices. In this paper a transport model for the amorphous phase of GST is investigated, based on the variable-range hopping model. The model is implemented into a Monte Carlo current-driven simulation of a test device made of a layer of amorphous $Ge_2Sb_2Te_5$ in contact with two planar metallic electrodes. The mechanisms governing electron transport within the device are discussed in relation to the variation of physical parameters, such as operating current, trap density, and coupling with the electric field inside the device.**

I. Introduction

Chalcogenide materials can suitably be exploited for manufacturing phase-change memory devices. Among them, the $Ge_2Sb_2Te_5$ (GST) compound has been identified as the most interesting material for industrial applications. Crystalline GST exhibits an almost Ohmic $I(V)$ curve; in contrast, amorphous GST (a-GST) shows a high resistance at low biases while, above a threshold voltage, a transition takes place from a highly resistive to a conductive state, characterized by a swift rise of the current along with a voltage snap back [1]. A clear and correct understanding of the threshold behavior of the amorphous phase is of the utmost importance for exploiting GST in the fabrication of innovative nonvolatile memories.

Experimental structural data and first-principle studies [2], [3] proved that amorphous chalcogenides are characterized by a large concentration of localized states. On the microscopic scale these states arise from structural defects of different nature, such as dangling bonds and vacancies, and they play the role of either donor- or acceptor-like traps. This picture suggests that an appropriate model for electric conduction in chalcogenides must rely on a trap-controlled transport process [4], [5], or, alternatively, on the generation-recombination mechanism via localized states [1].

II. The Physical Model

Our transport model is based on the generalization of the variable-range hopping theory (VRH). We assume here that a number of donor-like traps exist in the a-GST region and carriers can hop among them by tunneling.

Traps are positioned at random inside the a-GST. An energy-level, randomly chosen within a narrow band of width ΔE centered at the Fermi level, is attributed to each trap. The latter can host only one carrier at a time and is neutral when it is filled by an electron or it is positively charged when it is empty. In order to guarantee the electrical neutrality a number of acceptor states, always filled by carriers and not involved in the transport process, are also considered.

This scheme has been implemented by means of Monte Carlo simulations for a 3D device made of an a-GST layer sandwiched between two metallic contacts. These contacts are mimicked by two infinite "reservoirs" of carriers and empty states placed at the two opposite sides of the GST region. The reservoirs can provide electrons to be injected into the traps of the GST or host electrons coming from the GST at any time. The test device is sketched in Fig. 1.

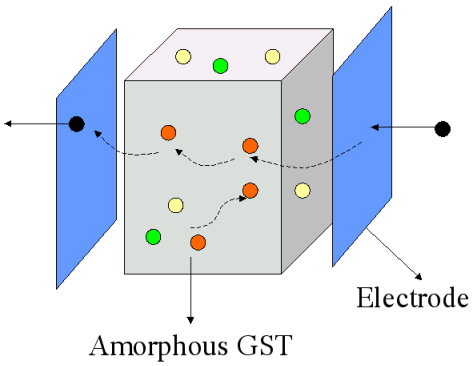

Fig. 1. Sketch of the device used in simulations. Electrons are injected into the right contact.

The transition rate S_{ij} for a carrier's hopping from an occupied site i to an empty site j is evaluated according to

the VRH theory [6]:

$$S_{ij} = \begin{cases} \nu_0 \, T_{ij} \exp\left[-\dfrac{\Delta\epsilon_{ij}}{k_B T}\right] & \text{if} \quad \Delta\epsilon_{ij} > 0 \\ \nu_0 \, T_{ij} & \text{if} \quad \Delta\epsilon_{ij} \leq 0 \end{cases} . \qquad (1)$$

Here, ν_0 is the attempt-to-escape frequency, $T_{ij}(R_{ij})$ is the transmission coefficient of the potential barrier between the sites i and j separated by the distance R_{ij}; $\Delta\epsilon_{ij} = \epsilon_j + e\varphi_j - \epsilon_i - e\varphi_i$ indicates the energy difference between the initial and final states, ϵ_i and ϵ_j being the intrinsic energy levels of traps i and j, and φ_i and φ_j are the values of the electric potential at the two sites. The transmission coefficient T_{ij} is related to the height of the potential barrier confining the carrier in the trap region.

In the original formulation [7], the energy barrrier between scattering centers does not depend on the electric field. However, this is clearly not realistic for the case at hand, where the electrostatic potential produces a non negligible variation of the energy barrier between two sites. Thus, T_{ij} is calculated as proportional to the overlap integral of two exponential tails of the electron wave functions in the barrier region, and results to be: $T_{ij} \propto e^{-2\alpha R_{ij}}$ where

$$\alpha^2 = \alpha_0^2 - \frac{m_0 e\beta}{\hbar^2}|\varphi_i - \varphi_j|, \qquad (2)$$

m_0 and β being the electron mass and a phenomenological parameter, respectively.

As reported above, the parameters contained in the model are linked to some properties of the material under investigation, and the sensitivity of the device on these parameters can be tested by means of appropriate numerical analyses that are presented in section IV-B.

III. Monte Carlo implementation

In order to investigate an S-shaped current-voltage characteristics, the standard voltage-driven Monte Carlo framework has been modified into a current-driven procedure. Specifically, the implemented Monte Carlo procedure can be summarized as follows:

1) Fill in the traps according to the equilibrium Fermi distribution. Set both the simulation time t_s and injection electron time t_I to zero.
2) Add an electron to the right contact and update t_I by $\Delta t_I = e/I$ (e and I being the electron charge and the prescribed current, respectively).
3) Evaluate the potential profile at each trap (or contact) site, and the voltage drop across the device, self-consistently with the actual trap-occupancy configuration.
4) Compute the transition rate for the any possible hopping process S_{ij}. The total hopping probability is evaluated as $S_{TOT} = \sum_i S_i$, $S_i = \sum_j S_{ij}$.
5) Generate a uniform random number r in order to update the simulation time of $\Delta t = -\ln r / S_{TOT}$. Check the new time: if $t_s + \Delta t > t_I$, the simulation time is set back to t_I and the procedure is cycled from step 2 without performing any further action, otherwise update t_s and go to the next step.
6) The starting trap i is chosen according to the probabilities S_i and, subsequently, the arriving trap j is selected according to S_{ij}. Contacts are considered as additional traps.
7) Perform the transition and update the trap-occupancy configuration; then if $t_s < t_{max}$ cycle from step 3.

The computation of the potential profile inside the device deserves care in order to preserve the correctness of the boundary conditions at the two metallic surfaces. The problem should be tackled and solved by the finite-element method. However, this approach is extremely demanding in terms of computational resources and has been replaced by an approximated quasi-3D electrostatic model. By means of the latter, trap-to-trap transition rates are evaluated considering charged traps like 3D point-like Coulomb centers, whereas for transition rates involving a contact, the trap potential is modelled as that of a charge sheet placed at the trap position and parallel to the contact, with total charge equal to the trap charge. Even though this approximation reduces the trap-electrode interaction to a 1D problem, the correctness of the bondary conditions at electrodes still holds true.

IV. Numerical results

A. Interpretation of the snap-back effect

The model presented above has been applied to a 3D region of a-GST (cross section $\sigma = 270$ nm^2 and length $\ell = 27$ nm) sandwiched between two planar electrodes, and the corresponding current density vs. voltage characteristics $J(V)$ has been compared to the experimental data [4]. Results are shown in Fig. 2; output values have been obtained as averages over 192 independent simulations to take into account statistical uncertainty. The simulation time in each step lasted from 0.1 to 1 ns depending upon the prescribed current, and it was adapted step-by-step to ensure that the stationary voltage values were reached within a variance of $2 \cdot 10^{-3}$ V.

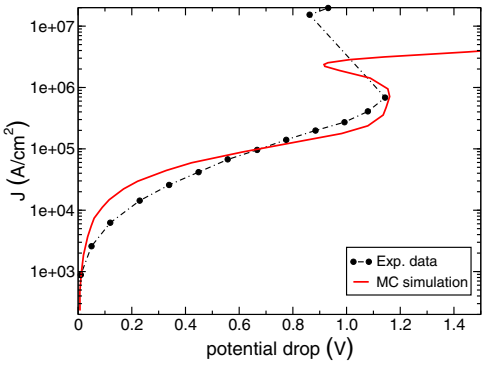

Fig. 2. Measured and simulated current density-voltage curves. Parameters used in the Monte Carlo simulation are: $N_t = 1.485 \cdot 10^{19}$ cm^{-3}, $\Delta E = 0.05$ eV, $\nu_0 = 1.35 \cdot 10^{13}$ s^{-1}, $\alpha_0 = 4.54 \cdot 10^6$ cm^{-1} and $\beta = 1/20$. Experimental data are taken from [4].

The simulated current-voltage characteristics shows the S-shape typical of the a-GST and is made of 1) a subthreshold region, which is divided into an Ohmic part at the lowest currents and an exponential part; 2) a negative differential-resistance region, where an increase of the prescribed current implies a decrease of the voltage drop across the device; and, finally, 3) by a fast increase of the voltage at the highest currents. In fact, we observe that in the upper part of the curve the model identifies a limiting current. This is rather unphysical, and indicates that a different transport process not considered in the present analysis, like, e.g., band conduction, must take place to sustain the current.

As far as the snap-back effect is concerned, both the threshold voltage (1.1 V) and current density ($7{\cdot}10^5$ A/cm^2) of the simulated $J(V)$ characteristics correspond to the experimental data for a prototype phase-change memory cell.

Addressing the physical details of the problem, the snap-back effect can be interpreted in terms of potential profile, transition rates and trap-occupancy (see Figs. 3-5).

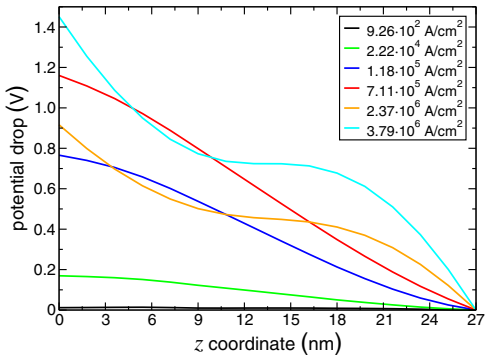

Fig. 3. Potential profile inside the device. Each line refers to a different applied current density J in the range $9.26{\cdot}10^2$- $3.79{\cdot}10^6$A/cm^2. Electrons enter the device from the right contact.

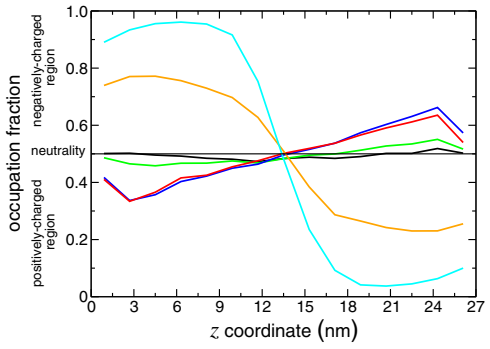

Fig. 4. Trap occupation fraction as a function of the axial coordinate of the device. The occupation fraction has been averaged over 192 simulations. Line colours correspond to the same situation as in Fig.3.

In the whole subthreshold region, up to $J \approx 10^5$ A/cm^2, the occupation fraction is around 0.5 keeping itself almost constant along the device, meaning that the space charge inside the device locally compensates. The voltage drop across the device is mainly due to charge accumulation at the two contacts: the

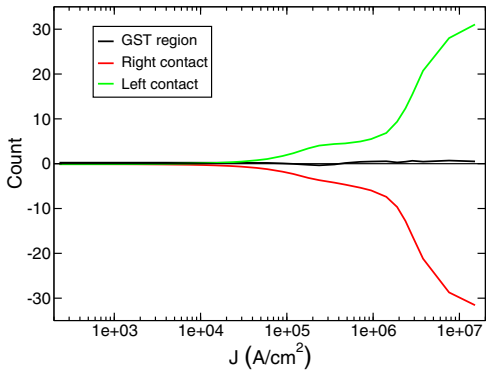

Fig. 5. Charge distribution inside the device and on the two contacts in the current density range $10^2 - 10^7$ A/nm^2. Electrons enter the device from the right contact.

internal electric field progressively increases with the current and lowers the energy barriers between traps, enhancing the occurrence of long-range transitions.

When the hopping process is not fast enough in trasferring carriers from the a-GST to the external circuit, charges are forced to accumulate close to the collecting contact. A counterfield originates inside the a-GST region and adds to the contribution coming from the two contacts. At this stage the internal potential profile is no more linear, and a more complex shape due to the superposition of different contributions is found. As a net effect, the potential drop decreases as the current increases.

In order to understand this effect, let us first consider that higher currents can be sustained only if more frequent transitions happen. This is achieved by emptying the region close to the injection contact, whose occupation number gets close to 0, and filling the region close to the collecting one (occupation number getting close to 1). The counterfield is enhanced to its maximum value, this hampering the carriers' flow between the contacts. As a result, the charge accumulates at the contacts and the potential drop between them quickly increases again. As anticipated, the model fails around the limiting current density $J \approx 5 \cdot 10^6$ A/cm^2, when some other transport mechanisms must gain importance and set in.

B. Effects of the parameters

Eqs. (1) and (2) are defined through a number of parameters that have a physical origin. The proposed model helps in understanding how they influence the $J(V)$ curve and, in turn, the features of a device.

The trap concentration N_t is of fundamental importance for the rise of the snap-back effect, as reported in Fig. 6. If the trap concentration is too low ($N_t < 5 \cdot 10^{18}$ cm^{-3}), the $J(V)$ curve monotonically increase; on the other side, the snap-back is present and enhanced by higher concentrations. Furthermore, we have found that the threshold voltage is reduced and the threshold current density J is increased by an increased trap concentration. It should also be pointed out that the slope of the subthreshold exponential region is not affected significantly by the variation of N_t, meaning that this region

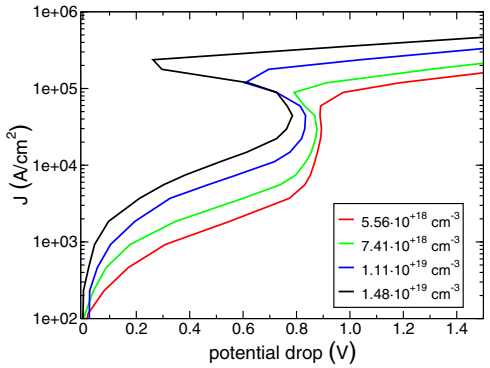

Fig. 6. $J(V)$ characteristics for different values of the traps density N_t in the amorphous region reported in the legend box. The other parameters used in the simulations are $\beta = 1/20$, $\nu_0 = 1 \cdot 10^{12}$ s^{-1}, and $\alpha_0 = 4.54 \cdot 10^6$ cm^{-1}.

of the $J(V)$ curve is more influenced by the other parameters, such as the energy barrier. These results confirm what already stated in the literature [4].

The shape of the $J(V)$ curve is also determined by the effect of α, defined through α_0 and β in eq. (2). The incorporation of a contribution due to the local field in the transition rates appears to be a key point, as reported in Fig. 7: when T_{ij} is kept independent of the local field, i.e. $\beta = 0$, the snap-back effect is absent. A small but non vanishing value of β makes the snap-back possible. The threshold voltage is highly sensitive to this parameter.

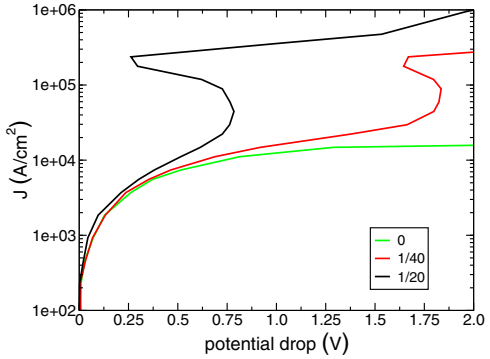

Fig. 7. $J(V)$ characteristic for three different values of β reported in the legend box. The other parameters used for the calculation are: $\nu_0 = 1 \cdot 10^{12}$ s^{-1}, $N_t = 1.48 \cdot 10^{19}$ cm^{-3}, and $\alpha_0 = 4.54 \cdot 10^6$ cm^{-1}.

Moreover, the characteristic tunnelling distance α_0^{-1}, which is an indirect measurement of the barrier height between two sites, also contributes to affect significantly the position of the threshold voltage and the slope of the exponential regime in the subthreshold region (see Fig. 8). As stated above, the snap-back condition is linked to the progressive lowering of α by the local field. It is thus evident that, for a fixed β, a larger value of α_0 requires a stronger potential to give the same effect. It should also be pointed out that both the threshold voltage and the subthreshold exponential slope are much more sensitive to β than to α_0; nevertheless the overall shape of the $J(V)$ curves is determined by the combined effects of both of them.

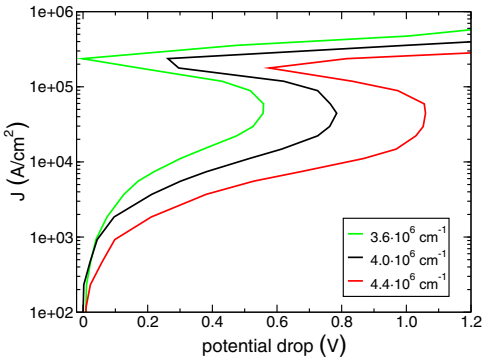

Fig. 8. Effect of the characteristic inverse tunnelling distance α_0 in the amorphous region on current-voltage curves. The other parameters used for calculation are: $\beta = 1/20$, $\nu_0 = 1 \cdot 10^{12}$ s^{-1}, $N_t = 1.48 \cdot 10^{19}$ cm^{-3}.

Finally, the attempt-to-escape frequency ν_0 is representative of the phonon spectrum of the GST layer; from literature data [6] it is of the order of 10^{12} s^{-1} or less. It is found that a change in ν_0 produces a rigid shift in the $J(V)$ curve proportional to the change itself along the current axis.

V. Conclusion

Charge transport has been investigated in a device made of a nanometric layer of a-GST sandwiched between two metal contacts. The theoretical framework provided by the analysis of a 3D transport in terms of variable-range hopping yields, without any further assumptions, a complete description of the mechanisms governing the threshold switching. The outcome of the investigation shows that the snap-back effect can be ascribed to the formation of domains of charges that modify the potential profile within the device and, in turn, the transitions rates.

Acknowledgment

This work has been carried out under the contract 34524/2007 of the Intel Corporation, whose support is gratefully acknowledged.

References

[1] A. Pirovano, A. L. Lacaita, A. Benvenuti, F. Pellizzer, and R. Bez, "Electronic Switching in Phase-Change Memories", *IEEE Trans. on Electron Devices*, vol. 51, no. 3, pp. 452-459, 2004.

[2] B. S. Lee, J. R. Abelson, S. G. Bishop, D-H. Kang, B. Cheong, and K-B. Kim, "Investigation of the optical and electronic properties og $Ge_2Sb_2Te_5$ phase change material in its amorphous, cubic, and hexagonal phases", *Journal of Applied Physics*, vol. 97, pp. 0935091-0935098, 2005.

[3] S. Caravati, M. Bernasconi, T. D. Kühne, M. Krack, and M. Parrinello, "Coexistence fo tetrahedral- and octahedral-like sites in amorphous phase change materials", *Applied Physics Letters*, vol. 91, pp. 1719061-1719063, 2007; M. Bernasconi, private communications

[4] D. Ielmini and Y. Zhang, "Analytical model for subthreshold conduction and threshold switching in chalcogenide-based memory devices", *Journal of Applied Physics*, vol. 102, pp. 0545171-05451713, 2007.

[5] D. Ielmini, "Threshold switching mechanism by high-field energy gain in the hopping transport of chalcogenide glasses", *Physical Review B*, vol. 78, pp. 0353081-0353088, 2008.

[6] N. F. Mott and E. A. Davis, *Electronic processes in noncrystalline materials*, Claredon Press, England: Oxford, 1961.

[7] A. Miller and E. Abrahams, "Impurity Conduction at Low Concentrations", *Physical Review*, vol. 120, no. 3, pp. 745-755, 1960.